JUNE 01 2015

Numerical analysis of aeroacoustic-structural interaction of a flexible panel in uniform duct flow

Harris K. H. Fan; Randolph C. K. Leung; Garret C. Y. Lam

J. Acoust. Soc. Am. 137, 3115–3126 (2015)
https://doi.org/10.1121/1.4921285

Numerical analysis of aeroacoustic-structural interaction of a flexible panel in uniform duct flow

Harris K. H. Fan, Randolph C. K. Leung,[a] and Garret C. Y. Lam
Department of Mechanical Engineering, The Hong Kong Polytechnic University, Hung Hom, Kowloon, Hong Kong, People's Republic of China

(Received 15 September 2014; revised 21 April 2015; accepted 3 May 2015)

Accurate prediction of the acoustics of fluid-structure interaction is important in devising quieting designs for engineering systems equipped with extensive flow duct networks where the thin duct wall panels are in contact with the flowing fluid. The flow unsteadiness generates acoustic waves that propagate back to the source region to modify the flow process generating them. Meanwhile the unsteady flow pressure excites the thin panels to vibrate, which in turn modifies the flow processes. Evidently a strong coupling between the fluid aeroacoustics and the panel structural dynamics exists. Such coupled physical processes have to be thoroughly understood; otherwise, effective quieting design is never achieved. This paper reports an analysis, using a time-domain numerical methodology the authors have recently developed, of the nonlinear aeroacoustic-structural interaction experienced by a flexible panel in a duct carrying a uniform mean flow. With no mean flow, the numerical results agree well with existing theories and reveal the physics of duct transmission loss. Four regimes of aeroacoustic-structural interaction are identified when the duct flow velocity increases from low subsonic to low supersonic values. Insight in the underlying physics of duct transmission loss at different velocities are highlighted and discussed.
 [http://dx.doi.org/10.1121/1.4921285]

[LC] Pages: 3115–3126

I. INTRODUCTION

Accurate prediction of noise generation by flow induced vibration is an important and challenging task in transportation and industrial problems. It is a major consideration in the quieting design of these systems that involve unsteady flows and vibrating flexible structures, such as those associated with power generation and ventilation in aircrafts, automotives, and domestic engineering installations. The noise generated by the operations of flow-moving machines, or by the turbulent flows in ducts, propagates through the ductworks in the systems and radiates from the duct outlets. Besides, the duct walls are commonly made of thin metal sheets. They are easily excited to vibrate by both turbulent flows and noise. Their vibration will generate additional noise to both interior and exterior of the flow ducts.[1] In such kind of problems, it is not uncommon to see that a complex coupling among the flow dynamics, acoustics, and structural dynamics is involved. The inherent noise generation mechanisms are indeed very complicated. A lack of the understanding of the interaction between these physical processes makes the noise control at source level become infeasible. Therefore many duct noise control solutions in current practice have to rely on the bulky absorptive installations, which are usually limited by the availability of space and weight requirement of the system designs.

Many researchers have developed different approaches in exploring the physics of flow-acoustics-structure interaction in situations commonly encountered in engineering systems. In some of the studies, the focus is put on the flow-structure interaction over the acoustic aspects. Carpenter and Garrad[2] developed a simple model for flow over a compliant surface supported on an elastic foundation for delineating the dynamics of different types of flow-induced surface instabilities. Lucey[3] studied the wave-bearing behaviour of a finite flexible plate in a uniform flow. He found that with certain combinations of flow and plate parameters, the plate may respond at frequencies other than that of the driver in the presence of flow. As he assumed an incompressible flow in his study, the corresponding acoustic generation was not resolved. Some researchers only looked at the interaction between an acoustic wave and vibrating structure. Frendi *et al.*[4] developed different coupling models for predicting the interaction between a panel and an incident wave in the absence of flow. He found that for this problem, a decoupled model was able to capture the panel response and its acoustic radiation with sufficient accuracy at relatively low computational cost. Huang[5] studied a duct noise control idea by installing a flexible panel in an otherwise rigid duct and provided theoretical predictions of the effects of the sound-structure interaction on duct acoustic transmission.

Other researchers are interested in studying the acoustic radiation driven by the flow-structure interactions. Clark and Frampton[6] demonstrated the importance of including aeroelastic coupling in modeling the structural acoustic response for interior noise control on modern aircraft. Schäfer *et al.*[7] attempted to solve the flow-acoustics-structure interaction of a flow past a thin flexible structure in a semi-open space. They calculated the flow-structure interaction using a numerical coupling of the solutions from a fluid dynamic solver and a structural dynamic solver and then determined the resultant acoustic field by adding the contributions from the

[a]Electronic mail: mmrleung@polyu.edu.hk

individual solver solutions. In that way, the acoustic solution was simply treated as a consequence of the flow-structure interaction.

All the aforementioned studies reveal that the current state of efforts in resolving the coupled interactions among flow dynamics, acoustics, and structural dynamics is still far from satisfactory. It merely remains in a stage in which the interaction between any two dynamics (e.g., flow-structure) is calculated, and the solution thus obtained is then used to deduce the remaining dynamical process as an effect. In some situations, such effect may be fed back to significantly modify the interaction creating it, but the determination this feed-back process is always lacking. Furthermore, the current approaches usually involve the use of three different numerical solvers for the three physical processes. Pairwise physical coupling requires three sets of extensive data exchange for the calculation of complete interaction. That way would inevitably lead to prohibitively high demands in computational resources, high programming difficulties as well as severe numerical errors arising from data extrapolation involved during exchange.

In this light, the goal of the present study is to use an simple yet accurate numerical methodology[8] to analyse the flow-acoustics-structure interactions encountered in real applications. The development of the methodology takes the view that typically a problem with such kind of interaction occurs within a domain composed of a compressible fluid and a flexible structure. It is logical to take an approach that accounts for the dynamical processes entirely in individual fluid and solid domains and then resolves their coupling. In this way all the unsteady flow motions (i.e., flow dynamics and acoustic wave motions) need to be solved together. From the point of view adopted, it is more appropriate to describe the interaction problem between acoustics and structural dynamics as an acoustic-structural interaction (ASI), whereas that involving the three dynamics altogether as an aeroacoustic-structural interaction (AASI). In this paper, we describe the key ideas in the formulation of the numerical methodology[8] in Sec. II, then demonstrate its capability and accuracy through calculating a canonical ASI of an in-duct flexible panel, and eventually extend the work to analyse the problem with a mean duct flow (i.e., the AASI problem), both in Sec. III.

We select the work by Huang[5] as our canonical ASI problem in which he proposed to flush-mount a finite length tensioned flexible panel in an infinite rigid flow duct for controlling low-frequency duct noise (Fig. 1). When a plane acoustic wave is propagating through the duct, the panel responds to vibrate, and the local distension in the vicinity of the panel thus created renders a local wave propagation speed far less than its isentropic value. The mismatch in the wave speed there leads to reflection and scattering of acoustic wave at the edges of the panel. The extent of reflection and scattering depends on the ASI occurring with the vibrating panel that eventually results in creating passbands and stopbands for the acoustic transmission. Assuming harmonic fluctuations and quasi one-dimensional variation along the duct for all dynamic quantities, Huang presented a detailed linear analysis in frequency domain of how various panel parameters influence the panel ASI and subsequently the transmission loss in the duct in case there is no flow. His results of the analysis are complete and provide a set of good reference for validating the numerical methodology proposed in the paper.

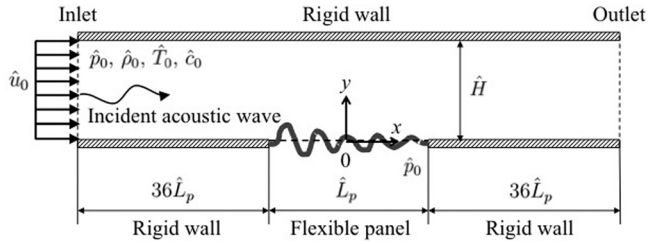

FIG. 1. Schematic configuration of the problem of interest (not-to-scale). The symbols with caret mean dimensional quantities.

II. FORMULATION OF NUMERICAL METHODOLOGY

The aforementioned hybrid approach of Schäfer *et al.*,[7] which drives the acoustic solution from the flow and the structural dynamics, is not appropriate for the present problem. It is because in a flow duct, the acoustic waves reflect at the duct walls and propagate back to the source region to alter the source flow dynamics and the panel vibration there. Furthermore, the coupling approach of Schäfer *et al.*[7] has to involve three pairwise channels for data exchange among three solvers. It inevitably involves much extrapolation of fluid and structural dynamic data that eventually leads to substantial loss of the accuracy information, especially those at high frequencies. To circumvent the deficiencies imposed by the hybrid approach, we adopt a numerical methodology that requires the minimum number of data exchange across the fluid-panel interface yet is able to maintain the accuracy of the solutions during time marching. In the numerical methodology, there are three key elements for calculating the AASI of the flexible panel. They are (i) the modeling of aeroacoustics of the fluid, (ii) the prediction of the panel dynamic response, as well as (iii) an accurate coupling strategy for the nonlinear interplay between the fluid aeroacoustics and panel structural dynamics. All these elements must be fully taken into account in the formulation of individual numerical solver, and each must be selected according to the configuration of specific problem of interest.

A. Aeroacoustic model

Acoustic motion is just a kind of unsteady flow motions that a fluid medium supports.[10] It is logical to adopt a numerical model for the fluid medium that calculates both the acoustic field and the unsteady flow generating it simultaneously. Otherwise, the inherent nonlinear interaction between these two fields cannot be properly accounted for in the calculation. This capability is particularly important in the calculations of the present problem. Acoustic waves arising from fluid-panel interaction undergo reflection at the duct walls. They may propagate back to alter the unsteady flows generating them and subsequently the panel vibration. Such

kind of phenomenon cannot be resolved using any hybrid aeroacoustic model in which the flow solution is used to drive the acoustic field but vice versa is not possible. Therefore in the present study, we adopt an aeroacoustic model based on direct aeroacoustic simulation (DAS) approach.[11,12] The aeroacoustic problem is governed by the two-dimensional compressible Navier–Stokes (N-S) equations together with the equation of state for calorically perfect gas. Choosing a reference length $\hat{L}_0$, a reference density $\hat{\rho}_0$, and a reference acoustic speed $\hat{c}_0$ from the problem, the N–S equations without source can be normalized and written in the strong conservation form as

$$\frac{\partial \boldsymbol{U}}{\partial t}+\frac{\partial(\boldsymbol{F}-\boldsymbol{F}_v)}{\partial x}+\frac{\partial(\boldsymbol{G}-\boldsymbol{G}_v)}{\partial y}=0, \tag{1}$$

where

$$\boldsymbol{U}=[\rho,\rho u,\rho v,\rho E]^{\mathsf{T}},$$

$$\boldsymbol{F}=[\rho u,\rho u^2+p,\rho uv,(\rho E+p)u]^{\mathsf{T}},\ \boldsymbol{F}_v=\frac{1}{\mathrm{Re}}[0,\tau_{xx},\tau_{xy},\alpha_x]^{\mathsf{T}},$$

$$\boldsymbol{G}=[\rho v,\rho uv,\rho v^2+p,(\rho E+p)v]^{\mathsf{T}},\ \boldsymbol{G}_v=\frac{1}{\mathrm{Re}}[0,\tau_{xy},\tau_{yy},\alpha_y]^{\mathsf{T}},$$

ρ is the density of fluid, pressure p, u, and v are the velocities in x and y direction, respectively, t is the time, $\alpha_x=\tau_{xx}u+\tau_{xy}v-q_x$, $\alpha_y=\tau_{xy}u+\tau_{yy}v-q_y$, normal and shear stress $\tau_{xx}=(2/3)\mu(2\partial u/\partial x-\partial v/\partial y)$, $\tau_{xy}=\mu(\partial u/\partial y+\partial v/\partial x)$, $\tau_{yy}=(2/3)\mu(2\partial v/\partial y-\partial u/\partial x)$, total energy $E=p/\rho(\gamma-1)+(u^2+v^2)/2$, heat flux $q_x=-[\mu/(\gamma-1)\mathrm{Pr}M^2](\partial T/\partial x)$, $q_y=-[\mu/(\gamma-1)\mathrm{Pr}M^2](\partial T/\partial y)$, the specific heat ratio $\gamma=1.4$, the Mach number $M=\hat{u}_0/\hat{c}_0=\hat{u}_0/\sqrt{\gamma\hat{R}\hat{T}_0}$, where the specific gas constant for air $\hat{R}=287.058$ J/(kg K), the Reynolds number $\mathrm{Re}=\hat{\rho}_0\hat{c}_0\hat{L}_0/\hat{\mu}_0$, and Prandtl number $\mathrm{Pr}=\hat{c}_{p,0}\hat{\mu}_0/\hat{k}_0=0.71$. There is a reason for our choice of solving the N–S equations for primitive flow variables rather than the convective wave equation for acoustic variables as adopted in another study for a similar problem.[13] To resolve the complex AASI of interest, we believe that we need to accurately capture not only the sound-panel interaction but also the nonlinear flow-panel interaction as well as their interplay at different Mach numbers. Because the convective wave equation may not capture the latter physics fully due to its linearization, we choose to solve the N–S equations instead. Once the primitive flow variable (e.g., the pressure p) is solved, its acoustic component can be readily found by subtracting its ambient value, i.e., acoustic pressure $p'=p-p_0$. Furthermore in all the expressions given in the preceding text, any symbol carrying a caret indicates its dimensional quantity; otherwise, it is treated as dimensionless. The same notation is adopted in the forthcoming discussion.

The DAS solver must be capable of accurately calculating the acoustic and flow fluctuations that exhibit large disparity in their energy and length scales especially at low Mach numbers. This imposes a strict requirement on the solver of being low dissipative and highly accurate. Conventionally, high order explicit finite difference schemes such as Bogey[14] are adopted in DAS. Recently, the conservation element and solution element (CE/SE) method[15] has been proven to be a viable alternative.[11] This numerical scheme takes an entirely different approach and concept from the conventional schemes (e.g., finite-difference). The construction of its numerical framework relies solely on the strict conservation of physical laws [Eq. (1)] and the emphasis on the unified treatment of flow fluxes in both space and time. In the present study, we adopt the CE/SE DAS solver given in Lam *et al.*[11] in which the authors showed the capability of solver in resolving complex aeroacoustic interactions at low subsonic to supersonic Mach numbers accurately. To avoid any contamination of erroneous waves reflected from the duct inlet and outlet, numerical anechoic terminations proposed by Lam *et al.*[11] are attached there.

B. Panel dynamic model

We assume membrane-type behaviour for the flexible panel and solve its dynamic response using a quasi one-dimensional flexible beam model spanning along x direction. Such model was taken by Huang,[5] and Choi and Kim[13] in their analytical ASI studies. Using the same set of reference parameters adopted in aeroacoustic model, the normalized governing equation for displacement $w=\hat{w}/\hat{L}_0$ of the panel in Fig. 1 can be written as

$$\rho_p h_p\frac{\partial^2 w}{\partial t^2}+C\frac{\partial w}{\partial t}-T_x\frac{\partial^2 w}{\partial x^2}=p-p_0, \tag{2}$$

where $\rho_p=\hat{\rho}_p/\hat{\rho}_0$ is the panel density, $h_p=\hat{h}_p/\hat{L}_0$ is panel thickness, $C=\hat{C}/(\hat{\rho}_0\hat{c}_0)$ is the panel structural damping coefficient, $T_x=\hat{T}_x/(\hat{\rho}_0\hat{c}_0^2\hat{L}_0)$ is the tensile stress resultants per unit length, p is the pressure imposed by the interior flow and p_0 is the pressure behind the panel. Note that this equation allows panel displacement up to $w/h_p\le 0.2$.[16,17] Equation (2) is solved using standard finite-difference procedures. The panel is initially discretized into a series of connected linear mesh of mesh size Δx (Fig. 2). All panel mesh points are located below the row of CE/SE solution points just next to boundary of fluid domain. All the spatial and temporal derivatives of w are approximated using standard central difference schemes,[18] whose details of derivation is referred to Leung *et al.*[8] The time-marching of the panel displacement from the jth to $(j+1)$th time step, with size Δt, is approximated as $w^{n,j+1}=[Cw^{n,j-1}\Delta t-2\rho_p h_p(w^{n,j-1}-2w^{n,j})+2\Delta t^2(p-p_0)+2T_x w_{xx}^{n,j}\Delta t^2]/(2\rho_p h_p+C\Delta t)$.

C. Boundary conditions and fluid-panel coupling

The boundary conditions for the duct fluid domain are prescribed as follows. Isothermal condition with temperature T_0 is specified on all solid surfaces. Sliding wall boundary condition, i.e., $v=0$, is prescribed on all rigid surfaces. The fluid boundary in contact with the vibrating panel are required to satisfy the tangency condition $(v-\dot{w})=0$ and the normal pressure gradient condition $\partial p/\partial y=\rho\ddot{w}$, which, respectively, ensure the continuity of velocity and momentum at the fluid-panel interface in marching the solution of

the problem. The flexible panel is pinned at its edges where the displacement and bending moment vanish.

At each time step, the vibrating panel displaces the fluid in its proximity. Recognizing the characteristic flow solution update processes in CE/SE method and the fact that the panel displacements are always very small compared to its thickness,[5] we account for the effects of panel displacement on the fluid domain with a simple technique that is derived in the spirit of immersed boundary method.[19]

In the CE/SE method, the solution points are not laid on the physical fluid domain boundary. The flow conditions at the physical boundary are manifested by placing ghost cells A_g behind the domain boundary as mirror images to boundary cells A_b (Fig. 2). Appropriate flow variables are specified at the ghost cells such that the desired flow conditions at the boundary are implicitly given by an interpolation between A_b and A_g. All flow variables other than the transverse velocity v_g in the ghost cell are set according to the sliding wall boundary condition specification of Lam *et al.*[11] For rigid duct boundaries, we set $v_g = -v_b$ so as to make $v = 0$ on the fluid-wall interface. For the vibrating panel, we assume that its displacement is smaller than the distance δ between A_b and the interface, and take the approximation $v_g = \dot{w}^n + (\dot{w}^n - v_b)(\delta + w^n)/(\delta - w^n)$, where v_b is the transverse velocity of A_b. Undoubtedly we need to pay attention whether our assumption is valid during the course of calculations. In all the calculations reported here, we found $w/\delta < 68\%$ consistently, which indicates that our proposed simplified technique performs well within its validity. For large displacement (i.e., $w > \delta$), the tangential panel velocity becomes significant, and the panel vibration starts to exhibit nonlinear behaviors. In this situation, a more elaborated panel dynamic model together with a procedure for updating fluid mesh deformation should be used.

When an aeroacoustic flow passes over a flexible panel, its associated pressure fluctuations will force the panel to vibrate. The vibrating panel then modifies the aeroacoustic boundary conditions, which subsequently changes the aeroacoustic forcing the panel receives. These two nonlinear processes occur simultaneously and give rise to the fluid-panel AASI. The fluid aeroacoustics and the panel response are coupled to each other through the normal pressure gradient condition (effect of flow unsteadiness on the panel response) and the tangency boundary condition (effect of panel response on the unsteady flow). Therefore a numerical scheme that allows seamless coupling of both effects is necessary for accurate prediction of the AASI involved. We conducted an evaluation of different fluid-panel coupling schemes with a similar problem of interest.[8] It was concluded that the one built along the idea of Jadic *et al.*[20] is able to give the solution accuracy required in resolving AASI correctly, so we choose it in all the calculations. A brief of the construction of the coupling scheme is given in Appendix A.

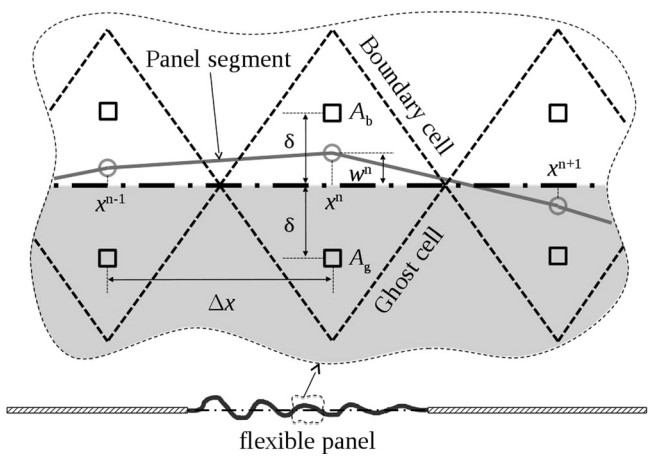

FIG. 2. Meshes around the nth panel mesh point at x^n on the fluid-panel interface. at fluid-panel interface. — ⊖ — ⊖ —, panel mesh segments; —·—·—, undeflected panel position.

III. RESULTS AND DISCUSSIONS

Although the numerical methodology is developed primarily for studying the nonlinear AASI of a flexible panel exposed to flow and acoustic excitations simultaneously, it would be informative to use it to calculate the ASI of the panel in the absence of flow first. There are two purposes. The first purpose is to assess how accurate the solutions the new methodology can produce through a comparison with existing frequency-domain theoretical results. The second is to further uncover any physics that could not be captured in the theory. In this regard, we take the same set of problem parameters Huang[5] studied, i.e., the duct width $\hat{H} = 100$ mm, panel density $\hat{\rho}_p = 1000\,\text{kg/m}^3$, the panel thickness $\hat{h}_p = 0.05$ mm, the tension $\hat{T}_x = 58.0601\,\text{N/m}$, and the frequency of incident wave $\hat{f} = 340$ Hz. We choose $\hat{L}_0 =$ panel length $\hat{L}_p$, ambient acoustic velocity $\hat{c}_0 = 340\,\text{m/s}$, time $\hat{t}_0 = \hat{L}_0/\hat{c}_0$, ambient density $\hat{\rho}_0 = 1.225\ \text{kg/m}^3$, ambient pressure $\hat{\rho}_0\hat{c}_0^2$, and ambient temperature $\hat{T}_0$ for the normalization of all flow and panel variables before solving Eqs. (1) and (2). The frequency of the incident wave $\hat{f}$ used is fixed at 340 Hz, which becomes $f = 0.1\ L_p/H$ after normalization. The computational domain is illustrated in Fig. 1. The duct sections upstream and downstream of the flexible panel are set equal to 36 L_p so as to ensure sufficient space for the generated acoustic waves to propagate. The Reynolds number Re is set equal to 10^{12} so that fluid viscosity effect is practically suppressed, and the flow in the calculation is essentially inviscid. Before actual calculations, the mesh and time step convergence need to be established. We use the chosen problem for the convergence study and a brief of the results is given in Appendix B. We adopt mesh II for all the calculations discussed in the forthcoming sections.

A. Acoustic-structural interaction

Huang[5] showed that an excited vibrating panel in duct reflects and scatters the incident acoustic wave p'_{inc} in the absence of mean flow. As a result of the ASI, the excited panel generates an acoustic wave, known as re-radiated wave $p'_{rer} = p' - p'_{inc}$, which destructively interferes with the incident wave downstream of the panel and results in a net reduction of transmitted acoustic energy. The energy reduction also depends on whether the panel is

structurally damped ($C \neq 0$) or not. The silencing performance is described by the transmission loss TL, in db, defined as

$$TL = -20\log_{10}\left|\frac{p'_{inc} + p'_{rer}}{p'_{inc}}\right|. \quad (3)$$

Huang showed that for a undamped panel, the TL behaves more or less an approximate regular function with L_p/H with its minimum values close to 0 db (Fig. 3, reported in Leung *et al.*[8]). The structural damping simply acts to enhance the TL particularly when the panel is long.

In general situation, any flow variable in the solution of Eq. (1) contains the fluctuations due to both the incident and re-radiated waves. We cannot determine the p'_{rer} directly from the numerical results. Therefore in addition to the actual calculation, we run an additional one in a synchronized manner on the propagation of p'_{inc} only within a rigid duct of the same size. We then subtract the rigid duct results from the results with flexible wall to obtain the p'_{rer}. In each calculation of TL, we first record the temporal evolutions of p'_{inc} and p'_{rer} at locations 20 L_p upstream and downstream, respectively, of the panel over one incident wave cycle. The locations are so selected that any higher-order duct mode, if generated from the panel, decays completely, and only plane waves can be detected. This requirement is consistent with the quasi one-dimensional propagation assumed in theory. Their root-mean-squared values are evaluated and substituted into Eq. (3) for the calculation of TL. A comparison of numerical TL with the corresponding theoretical predictions is given in Fig. 3. In all these calculations, there is a major change in the numerical setting from Huang's calculations. It is the way we include panel structural damping in our time-domain calculations. In Huang's analysis, he expanded the panel dynamics into the summation of N sinusoidal panel velocity eignmodes *in vacuo* and calculated the temporal variations of the modal coefficients for the panel response. The Nth panel modal damping coefficient can be estimated as, with normalization adopted for Eq. (1),

$$C = N\bar{C}\sqrt{T_x \rho_p h_p}, \quad (4)$$

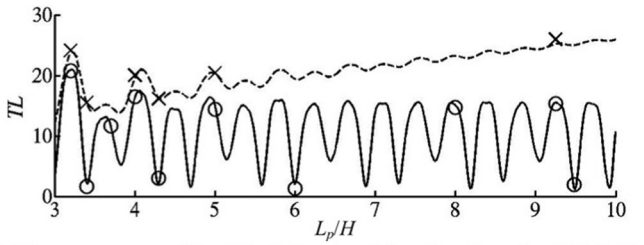

L_p/H		3.2	3.4	3.7	4	4.3	5	6	8	9.25	9.48
ΔTL	$C=0$	-0.1	-0.7	0.0	0.3	0.9	-0.2	-0.5	-0.3	-0.2	0.6
	$C=0.0196$	0.5	0.1		0.6	-0.1	0.1			0.8	

FIG. 3. Variation of transmission loss TL with panel length L_p/H. ———, theoretical result with undamped panel (Ref. 5); - - -, theoretical result with damped panel; ○, present numerical result with undamped panel; ×, numerical result with damped panel. The table shows the deviation ΔTL of numerical results from theory in all cases.

where the dimensionless $\bar{C}$ is a function of panel material property. We cannot apply the same damping coefficient directly in our time-domain calculations. Instead for the calculation of each damped case, we analyze and determine the dominant mode of corresponding undamped solution first. Then we substitute the dominant mode number N into Eq. (4) to set the value of C. Huang chose $\bar{C} = 0.2$, which gives $C = 0.0196$ in the present study. Figure 3 evidently shows that the present numerical results agree extremely well with the theory. The errors ΔTL lie well within 1 db. This shows that our present numerical methodology is able to capture the ASI of the flexible panel correctly.

We can better understand the mechanism of transmission loss through tracking the temporal evolution of the acoustic pressure fluctuations. Take the time-stationary solutions of the panels with $L_p/H = 3.2$ and 3.4, which, respectively, give high and low TL as examples (Fig. 3). The fluctuation pressure $p'/(p'_{inc})_{amp}$ of the total acoustic wave along the centerline (i.e., $y = 0.5$) of a duct with undamped panel $L_p/H = 3.2$ is shown in Fig. 4(a). In this figure, the recording of fluctuations starts at the moment when a maximum $p'_{inc}/(p'_{inc})_{amp}$ hits the leading edge of the panel and lasts one incident wave period t_1 ($= 1/f$). For easy comparison, the same recording time frame is applied to all forthcoming figures of the that show temporal pressure fluctuations. Upon exposure of the incident wave, the panel responds to vibrate and re-radiates toward both duct upstream and downstream with comparable amplitude [Fig. 4(c)]. The ASI supporting the re-radiation appears to start close to the leading edge of the panel at $x = -0.3$. The amplitude of the upstream p'_{rer} is same as the incident p'_{inc}. The two waves superimpose to form a complete standing wave the nodes of which are evident at $x = -1.79$ and -3.34. The downstream p'_{rer} has a weaker amplitude only 93% of the p'_{inc}. It adjusts its phase ϕ relative to the incident wave over the panel which eventually settles to a value close to -0.98π

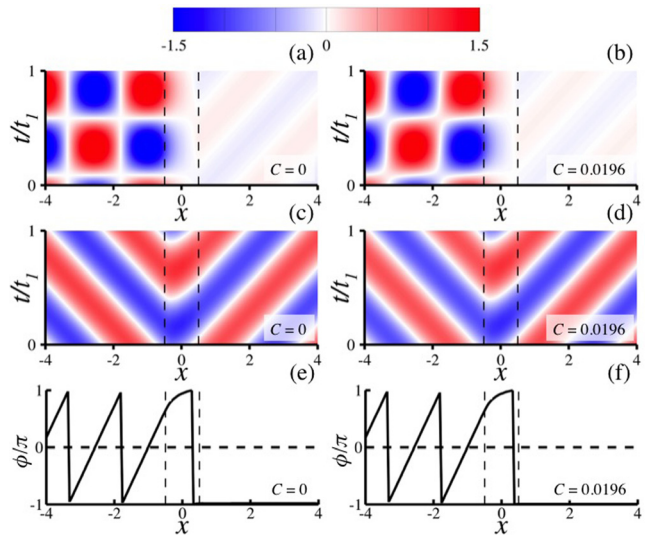

FIG. 4. (Color online) Acoustic response along the centerline of the duct with $L_p/H = 3.2$ within one incident wave period t_1. (a) and (b), the total fluctuation pressure $p'/(p'_{inc})_{amp}$; (c) and (d), the re-radiated waves $p'_{rer}/(p'_{inc})_{amp}$; (e) and (f), the phase shift of re-radiated wave relative to the incident wave. - - -, panel edges.

after passing $x = 0.34$ of panel trailing edge [Fig. 4(e)]. So it gives rise to an effective destructive interference along the duct and results in a high $TL = 20.9$ db. When the panel is damped, the presence of structural damping appears not to modify the ASI too much so similar acoustic pressure fluctuations prevail [Figs. 4(b), 4(d), and 4(f)]. The energy dissipation of panel damping reduces the amplitudes of the upstream and downstream p'_{rer} to 89% and 94% of the incident wave. Also, as the ϕ is much closer to -0.99π than in the undamped case, the destructive interference becomes more effective. Therefore the TL is further increased to 24 db.

The ASI of the panel appears to change substantially when the panel length is increased only by 6.2% to $L_p/H = 3.4$. Figures 5(a) and 5(c), respectively, show the evolution of $p'/(p'_{inc})_{amp}$ and $p'_{rer}/(p'_{inc})_{amp}$ of the undamped panel. In this case, the p'_{rer} shows a strong preference toward downstream of the panel. The amplitude of the upstream propagation is only 50% of the incident so a partial standing wave forms [Fig. 5(c)]. The nodes are shifted toward the panel to $x = -1.49$ and -2.94. The downstream p'_{rer}, with an amplitude of 138% of the incident wave, now begins approximately at the center of the panel ($x = 0.1$) and gives a higher $\phi = -0.8\pi$. These changes altogether destroys the destructive interference in the downstream duct section effectively so the TL is reduced sharply to only 1.8 db (Fig. 3). When the panel is damped, ϕ goes back to -0.97π, which promotes the destructive interference again [Fig. 5(f)]. Note that in this case, the amplitudes of upstream and downstream p'_{rer} are 74% and 112% of the incident. The stronger downstream p'_{rer} further enhance the destructive interference so a high $TL = 15.8$ db is resulted.

To ascertain the capability of the present numerical methodology in capturing the panel response under ASI, we capture and analyze the variation of the panel velocity over one incident wave period. Figure 6(a) shows the wavenumber spectrum of the panel mobility, which is defined as $Y_k = (\dot{w}(k))_{rms}/(p'_{inc})_{rms}$ where k is the wavenumber of a panel with $L_p/H = 5$ without damping. Here we first use standard spatial FFT procedure to obtain the $\dot{w}(k)$ spectra at all time instants within one period and then evaluate their *rms* spectrum over time. Using Huang's theoretical data, we calculate and include the modal mobility Y_k (N) in the figure as crosses for comparison. The panel response dominates the spectrum within a narrowband centered at $k = 6$ corresponding to the 12th panel mode. Figure 6(b) shows a comparison of the distribution of mobility $Y_x = (\dot{w})_{rms}/(p'_{inc})_{rms}$ along the panel with that derived from the theoretical results. Both sets of results show excellent agreement. They show the leading edge response is stronger than elsewhere. Furthermore we attempt to expand our numerical panel responses using the same set of eigenwave modes Huang adopted. The corresponding modal $Y_k(N)$ is shown as circles in Fig. 6(a). It can be seen that all the numerical $Y_k(N)$ overlap with the theoretical values except the one at the peak.

These evidence firmly shows the high accuracy the present numerical methodology can reach as well as the necessity of a coupled calculation for solving ASI problems. The maximum deviation of numerical Y_k and Y_x amplitudes from the theoretical values are 5.9% and 4.9%, respectively. All these differences may be attributed to the stronger fluid-damping induced on the panel response due to the lack of inclusion of the reaction force imposed on the fluid induced by the panel motion in the theory. Generally these two figures clearly

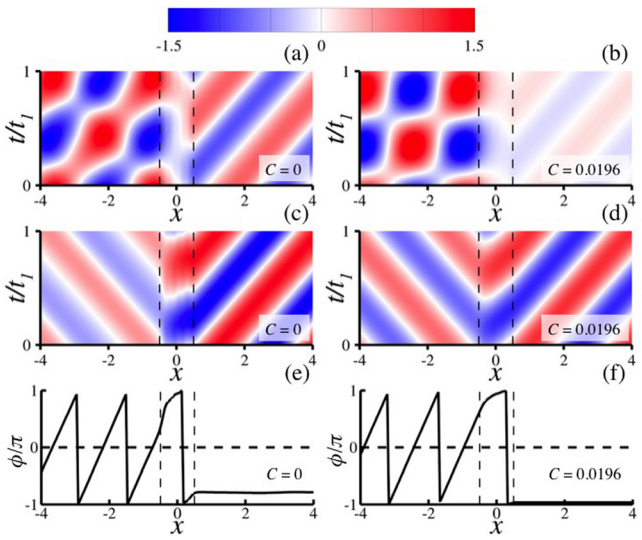

FIG. 5. (Color online) Acoustic response along the centerline of the duct with $L_p/H = 3.4$ within one incident wave period t_1. (a) and (b), the total fluctuation pressure $p'/(p'_{inc})_{amp}$; (c) and (d), the re-radiated waves $p'_{rer}/(p'_{inc})_{amp}$; (e) and (f), the phase shift of re-radiated wave relative to the incident wave. - - -, panel edges.

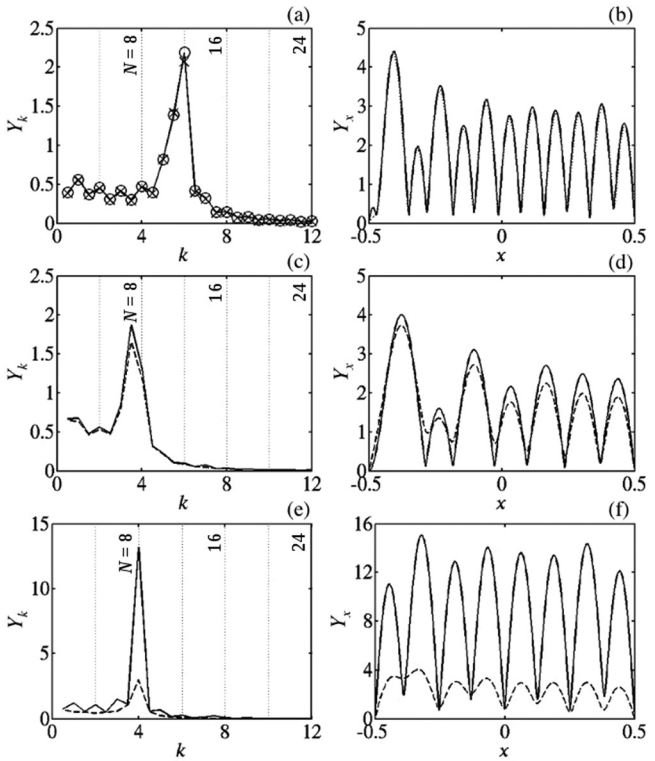

FIG. 6. Panel responses. Left column, panel mobility spectra Y_k; right column, the distributions of panel mobility amplitude Y_x. (a) and (b), $L_p/H = 5$; ○, present numerical panel mode number N; ×, theoretical panel mode number (Ref. 5); …, theoretical undamped Y_k. (c) and (d), $L_p/H = 3.2$; (e) and (f), $L_p/H = 3.4$. (c) through (f), ———, $C = 0$; - - -, $C = 0.0196$.

indicate the present numerical methodology is able to capture the panel responses accurately. It is interesting to note in Fig. 6(b) that the present numerical methodology captures all the 12 peaks, as predicted in the theory, including the very weak first peak at $x=-0.48$ with $Y_x=0.4$, which does not show up in the solution of Huang[5] [his Fig. 4(b)]. The observation may be attributed to one fundamental difference between his and present works. In the theory, a harmonic temporal dependence is assumed for all fluctuating quantities. Such assumption effects the capture of the relatively strong harmonic ASI solutions but the capturing of any transient or weak dynamics may not be effective. On the contrary, there is no such restriction in the present methodology, so the weak first peak in Fig. 6(b), the magnitude of which is less than 10% of the others, can still be captured. In fact, we got the same weak peak back from the calculation of the same problem using a loose fluid-panel coupling approach.[8] That further supports an assumed harmonic dependence is too restrictive for resolving the ASI problem completely.

Figures 6(c) and 6(d) show the Y_k spectra and Y_x distributions for the panel with $L_p/H=3.2$. The panel response dominates within a narrowband centered at $k=3.5$ (i.e., $N=7$). The structural damping serves to reduce its amplitude by only 14%. Again the leading edge response is the strongest. Figures 6(e) and 6(f) show the same quantities for $L_p/H=3.4$. In this case, the peak Y_k response appears to be seven times stronger than that of the shorter panel, but it can be significantly suppressed with the structural damping. The strongest response is still close to leading edge, but its amplitude is higher than elsewhere mildly. Generally stronger panel response tends to re-radiate stronger acoustic wave to duct downstream. However, as explained earlier, the eventual destructive interference and subsequently the *TL* there depends critically on the its phase ϕ induced by the ASI as well as the structural damping if any.

B. Aeroacoustic-structural interaction

We continue to study how the flexible panel in Fig. 1 interacts with simultaneous flow and acoustic excitations and its AASI response. We keep the same incident acoustic wave and introduce the simplest kind of the flow excitation, i.e., an uniform mean flow with Mach number M along the same direction. The flows with substantial velocity gradient (e.g., boundary layer flow, fully developed flow, etc.) are left to later studies because they tend to promote flow instability, which makes the analysis more difficult. The capability of the numerical methodology in capturing AASI was established, and a brief of the validation is described in Appendix C.

In the present study, we select an undamped panel with $L_p/H=3.2$ and study its variation from low subsonic M to supersonic $M=1.2$. The mean flow creates an additional dimension to the incident wave for the excitation acting on the flexible panel. It is enlightening to analyze and study the nonlinear impact on the panel response upon a change from ASI to AASI. An overview is given in Fig. 7. We obtain the wavenumber spectra of the time-stationary panel dynamic solutions of all cases and derive the panel modes in the same way as in Sec. III A. The variation of the panel mobility Y_k with M is illustrated in Fig. 7(a). Here we express the spectra in terms of mode number N, rather than k, for easier comparison with the ASI case. From a careful observation, we can discern four distinct regimes for the panel response with respect to M. In the first regime where $M\le 0.1$, the panel response essentially dominates within a narrowband centered at the same panel mode (i.e., $N=7$) as in the no flow case. The bandwidth widens when M increases, but the peak amplitude simultaneously reduces. At $M=0.1$, the modal amplitudes at $N=6$–8 are comparable, which signifies a substantial change of the panel response characteristics. The second regime covers $0.1<M\le 0.5$, which gives a substantial change in AASI. For instance, when $M=0.3$, the Y_k distribution transforms from an unimodal to a bimodal pattern with a strong modal band at $N=4$ and a weak one at $N=10$ [Fig. 7(b)]. As M increases further, the lower modal band strengthens and migrates toward $N=0$. At the same time, the higher modal band moves away from the lower band but it gets weaker. Another substantial change in AASI prevails in the third regime that covers $0.5<M<1$. The lower band settles at $N=1$ as M equals 0.8. The band widens mildly when M increases to 0.9. In the fourth regime in which the flow velocity becomes sonic or faster, there is only a single mode at $N=1$. The bimodal pattern revealed in Fig. 7(a) suggests that as a result of the nonlinear AASI, two types of flexural waves emerge in the panel response. For a better understanding of their propagation characteristics, we capture the panel response in one incident wave period and apply the technique proposed in Lam *et al.*[12] to the recorded data to obtain the frequency/wavenumber distribution of $\dot{w}$ from which the propagation velocities c_B of the flexural waves are readily determined. It is found that whenever the mean flow is subsonic, there are the two flexural waves propagating in opposite directions on the panel [Fig. 7(b)]. The flexural waves associated with lower modal bands propagate

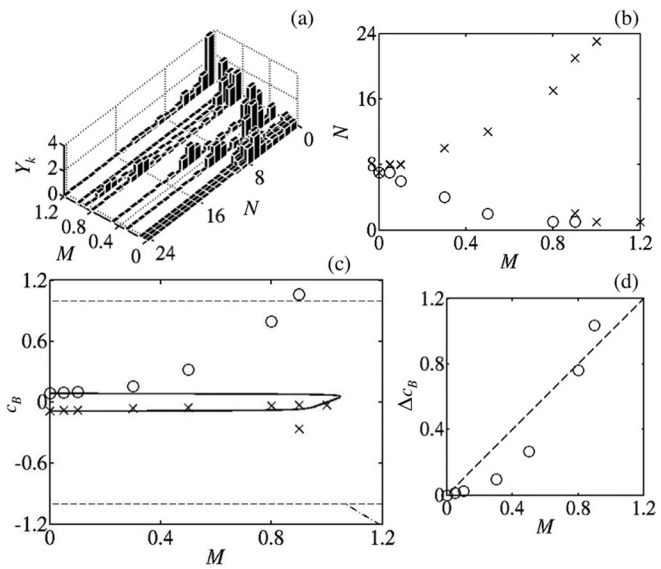

FIG. 7. Panel responses. (a) Variation of Y_k spectra with M. (b) Distribution of dominant modal peaks. (c) Distribution of flexural wave velocity c_B. ———, the subsonic branch; –·–·–, the first mode of supersonic branch; · · ·, $c_B=1$. (d) The difference between the two opposite flexural wave velocities. In (b) and (c), ○, $c_B>0$; ×, $c_B<0$.

toward downstream, but those with higher bands propagate against the flow direction. When $M=0.9$, an extra flexural wave with $N=2$ appears. When $M\geq 1$, only the upstream propagating flexural waves exist.

Choi and Kim[13] carried out an analysis for the same setup as in the present problem. They derived a general equation for the flexural wave dispersion characteristics in an infinitely long panel with the effect of mean flow taken into account. It is given in the following equation after normalization,

$$\rho_p h_p \omega - iC - T_x \omega / c_B^2 = iZ_f, \tag{5}$$

where $i^2=-1$, $\omega=2\pi f$, the fluid impedance Z_f equals $-i\rho\omega\cot(k_y)/k_y$ when $c_B>1$ (supersonic branch), and $i\rho\omega\coth(|k_y|)/|k_y|$ when $c_B<1$ (subsonic branch) with $k_y=\omega\sqrt{(1-M/c_B)^2-1/c_B^2}$. Note that here the descriptions supersonic, or subsonic, indicate when the flexural wave velocity propagates faster, or slower, than the ambient acoustic velocity in fluid domain. It is different from the definition of M, which measures the mean flow velocity relative to the ambient acoustic velocity. For the present panel of interest, we solve Eq. (5) to determine the eigenwave velocities at different M, and compare the results with the flexural velocity resolved from the frequency/wavenumber distribution [Fig. 7(c)]. In this figure, only the first two theoretical eigenwave modes are shown.

Roughly speaking, the same four regimes defined earlier are evident in the variation of flexural wave characteristics with M. When there is no mean flow, the flexural waves simply propagate with the first eigenwave velocities. Only a minor velocity shift is observed with an increase in M, up to 0.1, which shows that the effect of AASI is not strong in this regime. The velocity shift becomes prominent in the second regime. The downstream propagation velocity appears to grow significantly with M as it aligns with the mean flow direction. The upstream propagation, however, slows down slightly from its first eigenwave velocity. Notwithstanding these velocity changes, the modal mobility Y_k still exhibits a regular pattern along the panel [Figs. 8(a) and 8(b)]. The velocity shifts appear to strengthen in the third regime. Substantial changes in propagation characteristics are observed at $M=0.9$. In this situation, the downstream propagation becomes supersonic (i.e., $c_B>1$). An additional subsonic upstream propagating wave with $c_B=-0.27$ emerges. When the mean flow becomes sonic ($M=1$), the downstream propagation stops and only two upstream propagation modes are possible. One of them is close to the theoretical eigenwave velocity but another takes up a much higher $c_B=-16$ [not shown in Fig. 7(c)] with mode shape $N=1$ [Figs. 7(a) and 8(c)]. In the last regime, the c_B slows down to -5.3 (again not shown) when the mean flow takes a supersonic $M=1.2$ in which the regularity of Y_k distribution is completely lost [Fig. 8(d)].

It may be argued that the emergence of bimodal flexural wave pattern in the panel response just manifests the Doppler effect of the acoustically induced excitation under the action of mean flow. In this situation, the difference between the two opposite flexural wave velocities Δc_B should bear a linear relationship with M. However, Fig. 7(d) shows that this is not the case with the calculation results. The supersonic flow case is not included as the panel there has only one wave. The difference is less than M for low subsonic flow, passes over at moderate $M\sim 0.8$, and becomes higher with high subsonic M ($\Delta c_B=1.04$ at $M=0.9$). Such trend clearly indicates the nonlinearity that AASI imposes on the panel dynamics. It may also be argued that the bimodal pattern may be a result of the Kelvin–Helmholtz instability of an inviscid incompressible uniform flow over a long compliant surface as indicated in the theories of Miles[21] and Huang.[22] Their theories state that instability emerges whenever the flow pressure acting on the flexible panel becomes stronger than the restoring force the flexible panel in the flow-surface interaction. In our normalization, this occurs when $c_B^2<M^2/\rho_p$. The condition is, however, not satisfied in all our cases showing bimodal patterns, so the bimodal pattern should not be a result of the Kelvin–Helmholtz instability. Comparing to their theories, the assumption of fluid incompressibility is relaxed in the present study. It may be further argued that it is the effect of fluid compressibility that triggers the bimodal pattern. The underlying mechanism has not been clearly understood yet, so a further study is needed.

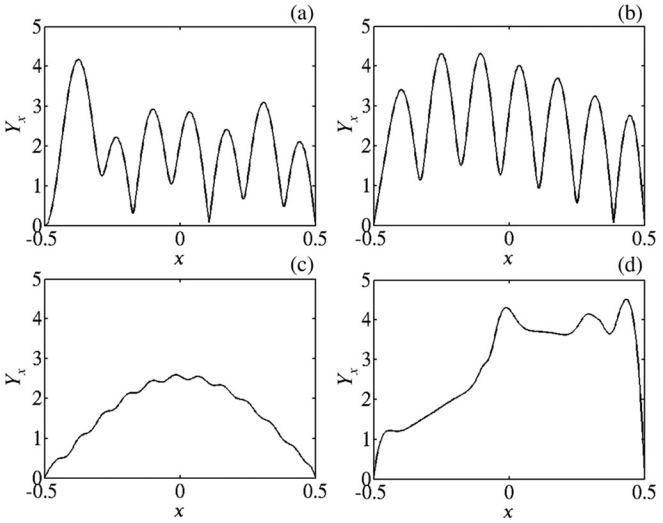

FIG. 8. Distributions of Y_x at different M. (a) $M=0.1$; (b) $M=0.5$; (c) $M=1$; (d) $M=1.2$.

The determining effects of AASI on the flexural characteristics and panel modal response impose a great impact on the acoustic transmission along the duct. Figure 9(a) shows the amplitudes of the upstream and downstream re-radiated wave at different M. The upstream p'_{rer} seems to be prominently affected by the convective effect of the flow. It grows with flow velocity until $M=0.8$. Afterward it reduces sharply down to the zero at $M=1$ and maintains zero with supersonic flow. On the other hand, the downstream p'_{rer} appears to be strongly influenced by the panel dynamics. In fact we can still observe the variations of its amplitude can be described with the same four regimes identified with panel response (Figs. 7 and 8). The amplitude shows approximately step wise increase in the first three regimes within subsonic M and eventually drops linearly with M when the

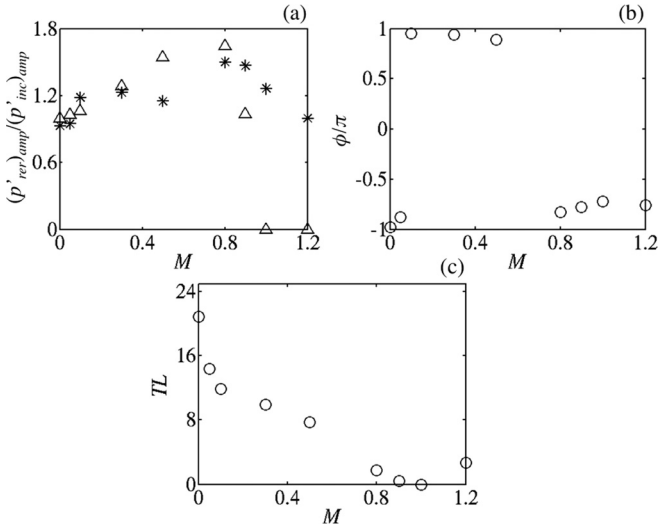

FIG. 9. Variations of acoustic response with M. (a) Re-radiation amplitude. Δ, upstream radiation; *, downstream radiation. (b) Phase shift of the downstream re-radiation relative to the incident wave. (c) Transmission loss.

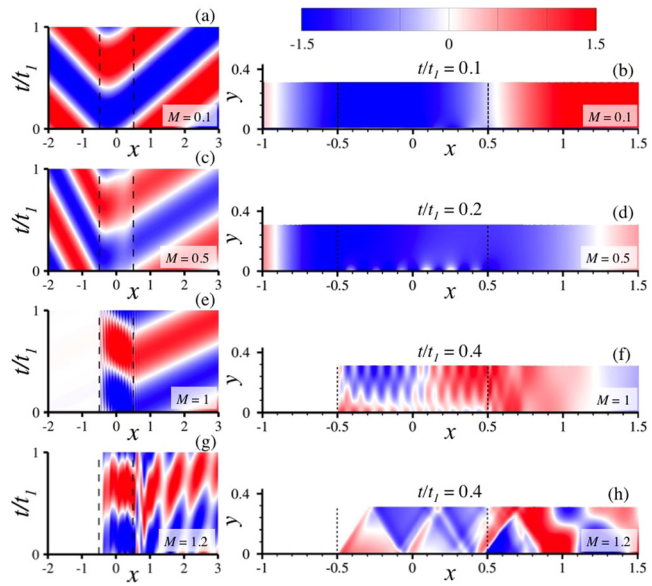

FIG. 10. (Color online) Re-radiation at different M ($L_p/H = 3.2$). Left column, p'_{rer} along the centerline of the duct. Right column, snapshots at selected t_1.

flow becomes supersonic. In addition, the AASI effects cause a nonlinear variation of the phase ϕ between the downstream re-radiation and the incident wave [Fig. 9(b)] and thus modify the destructive interference in duct downstream of the panel.

An overview of the AASI on TL is shown in Fig. 9(c). Generally the AASI acts to suppress the TL the magnitude of which drops with M in a nonlinear manner. The same four regimes as observed with panel response are evident in the figure. The TL drops with a rate of ∼90 db per unit of M within the range $M \leq 0.1$, of ∼10 db over $0.1 < M \leq 0.5$, and then of ∼16 db for $M > 0.5$. It vanishes with a sonic mean flow and grows again with a rate of ∼13 db per unit of M up to $M = 1.2$. The emergence of the TL trend can be explained with the downstream re-radiation patterns illustrated in Fig. 10. As observed in Fig. 10(a) the p'_{rer} at $M = 0.1$ shows high resemblance to the case without mean flow [cf. Fig. 4(c)]. That means the AASI induced in this case operates in a similar way as the pure ASI. Although the flow convection increases the deviation of ϕ from π by a small amount [Fig. 9(b)], it is sufficient to distort the standing wave pattern upstream of the panel and make the destructive interference downstream less effective. As a matter of fact, perfect destructive interference is never achieved under AASI. So the TL drops from 20.9 db at $M = 0$ to reach 11.9 db at $M = 0.1$, weakens further to 7.7 db at $M = 0.5$ at which the flow convection effects enhances [Fig. 10(c)], and then practically vanishes at $M = 1$. It is worthwhile to note that as long as the mean flow is subsonic, the p'_{rer} generation is confined in the proximity of the excited panel and will propagate away as clean plane waves at the panel leading and trailing edges [Figs. 10(b) and 10(d)]. Comparing with Figs. 8(a) and 8(b), the panel location showing the strongest modal response is responsible for the strongest generation. When the flow becomes sonic, p'_{rer} is able to propagate only in downstream direction. All the excited panel vibrating modes shown in Fig. 8(c) act as the sources of re-radiation. Once generated, the p'_{rer} will undergo multiple reflections between the upper duct wall and the vibrating panel and form a partial standing wave across the duct width [Fig. 10(e)]. Part of its energy propagates away as a plane wave mixed with contribution from the excited first higher-order duct acoustic mode [Fig. 10(f)]. The higher-order mode radiation decays rapidly and a clean plane wave emerges at $x \sim 1.3$. Although the eventual plane wave in p'_{rer} is 27% stronger than the incident wave, their resultant wave gives an amplitude identical to the incident wave with their ϕ given in Fig. 9(b), so $TL = 0$.

A new AASI phenomenon emerges at $M = 1.2$ [Figs. 10(g) and 10(h)]. In this case, a shock forms and reflects after hitting the upper duct wall at $x \sim -0.3$. The multiple reflection of oblique shock waves persists up to $x \sim 0.9$. The occurrence of this phenomenon can be explained as follows. Under the action of AASI, the displacement of the vibrating panel effectively produces a weak obstruction to the passage of the mean flow. When the supersonic mean flow approaches the obstructing panel vibration, it is forced to change its direction for satisfying the tangency boundary condition (Sec. II C) and consequently creates a weak oblique shock at the panel leading edge. Such flow features resemble that occur in a steady isentropic supersonic flow passing over a wedge with a half-angle θ_{wedge} (Ref. 23) and the flow Mach number, determines the shock angle in response to flow direction change. Assuming the effective θ_{wedge} in the present case is equal to the *rms* value (= 0.052°) of the panel deflection over one incident wave period, the theory of gas dynamics predicts an effective shock angle of 56.54° at $M = 1.2$. From the present numerical results, we determine the *rms* shock angle to be 57.28°. The close agreement between the numerical and theoretical shock angle confirms the obstruction effect of panel vibration. The deviation may be attributed to the phase difference of p'_{rer} generation along the vibrating panel. One may argue that the panel vibration can be viewed equivalently as a collection of acoustic point sources for p'_{rer} generation laid along an unexcited panel. The shock waves are just the

accumulation of upstream propagation p'_{rer} due to the Doppler effect of the supersonic mean flow. From this view, we calculate the shock angle to be 56.44°. Its relatively larger deviation from the numerical results firmly establishes the panel displacement really matters in the present problem and highlights its role in the AASI at high flow velocity. From Fig. 10(h), the oblique shocks tend to strongly excite the first higher-order duct mode in p'_{rer} which decays completely beyond $x = 20$. It then also produces a p'_{rer} plane wave but its amplitude is weaker than in the $M = 1$ case. It is interesting to note that the fluid-loading induced by the shock waves within $-0.5 \le x \le 0.1$ is so strong that only a limited modal vibration is possible around panel leading edge [Fig. 8(d)]. The modal vibration near the panel trailing edge gets stronger due to weaker fluid-loading induced by the shock waves within $0 \le x \le 0.45$ and appears to contribute most to the p'_{rer} radiation far downstream.

IV. CONCLUSIONS

In this paper, we have presented a numerical analysis of the aeroacoustic-structural interaction of a flexible panel installed in a duct carrying a uniform mean flow using a time-domain numerical methodology. The methodology consists of three key specific requirements: (i) an accurate description of the aeroacoustics of the duct flow, (ii) an accurate modeling of the panel dynamic response, and (iii) a seamless coupling strategy for capturing the interplay between these two physical processes. There are two advantages with the methodology over the existing methods for similar problems. It allows us to calculate the interaction between the acoustics, unsteady flow as well as the panel dynamics of the problem in a seamless manner in time domain so the inherent nonlinearity of the interaction can be more accurately captured than with existing frequency-domain methods. As it involves only two solvers for three physical processes in the problem, it suffers less interpolation errors than those methods requiring three individual solvers that exchange data in pairs. This feature helps maintain sufficient numerical resolution in the calculation over a much wider frequency range of the complex aeroacoustic-structural interaction. Calculations of the acoustic-structural interaction of both undamped and damped panels in the absence of flow were carried out. The details of the panel structural responses and the transmission loss induced by the acoustic/aeroacoustic-structural interactions are captured. The excellent agreement between the numerical results with theories firmly establishes the capability of the numerical methodology. The physical mechanisms responsible for the production of transmission loss are detailed. We further study the panel aeroacoustic-structural interactions with low subsonic to low supersonic mean flows. The numerical results reveal that the flow Mach number plays a critical role in determining the extent of aeroacoustic-structural interaction. Four regimes with respect to Mach number are identified. In the three regimes with subsonic Mach numbers, the interaction tends to reduce the transmission loss monotonically down to zero when the flow becomes sonic. A description of the nonlinear coupling between the panel dynamic and aeroacoustic responses responsible for such trend is given. The transmission loss goes up again in supersonic regime in which a completely different kind of aeroacoustic-structural interaction mechanism prevails.

ACKNOWLEDGMENTS

The authors gratefully acknowledge the support given by the Research Grants Council of Hong Kong SAR Government under Grant Nos. PolyU 5230/09E and PolyU 5199/11E.

APPENDIX A: FLUID-PANEL COUPLING SCHEME

Figure 11 show a schematic illustration of the fluid-panel coupling scheme we adopt in the present study. Here aeroacoustic model (AAM) and panel dynamic model (PDM) are defined in Secs. II A and II B, respectively. In the calculation at the jth time step, initial solution estimates $\boldsymbol{U}_{ie}$ and $\boldsymbol{W}_{ie}$ are first evaluated from the AAM and PDM using the solutions at (j-1)th time step as input. The estimates are then fed into a predictor-corrector procedure in which the errors in satisfying of both tangency condition and normal pressure gradient condition are minimized in an iterative manner. Essentially, an interim aeroacoustic estimate $\boldsymbol{U}_{k+1}$ is obtained with an predicted boundary condition $\lambda \boldsymbol{W}_k + (1 - \lambda)\boldsymbol{W}_{k-1}$, where λ is the relaxation factor.[24] Then an interim estimate $\boldsymbol{W}_{k+1}$ is obtained with an predicted forcing from $\lambda \boldsymbol{U}_{k+1} + (1 - \lambda)\boldsymbol{U}_k$. If the relative errors between $\boldsymbol{W}_k$

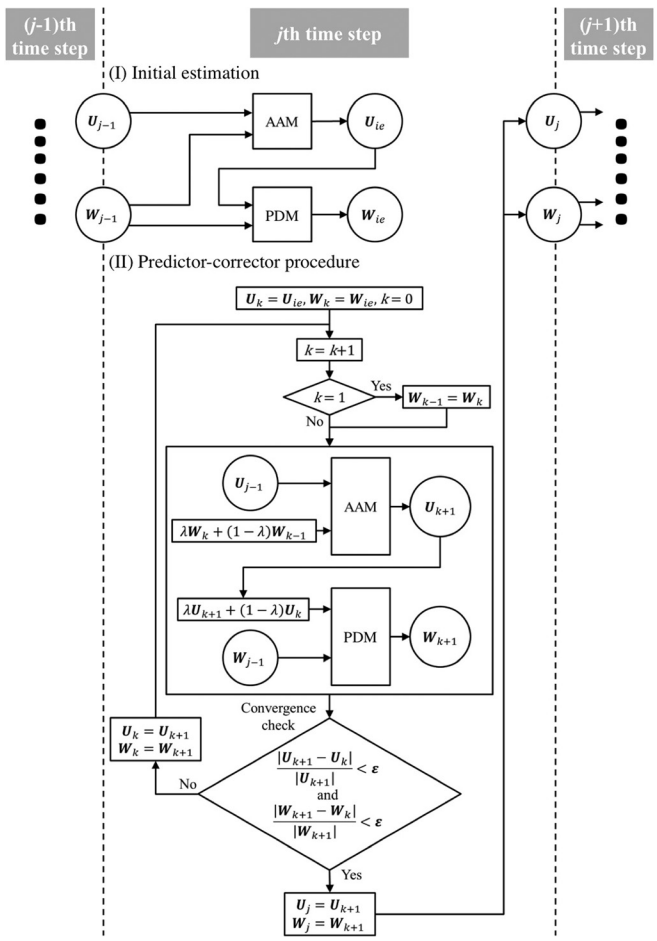

FIG. 11. Calculation procedure of the iterative coupling scheme. AAM, aeroacoustic model; PDM, panel dynamic model. Here $\boldsymbol{W} = [w, \dot{w}, \ddot{w}]$.

TABLE I. Mesh designs. The mesh stretching function, $F_i\,(\Delta x_{min}, \Delta x_{max}, B) = 0.5\,(\Delta x_{max} - \Delta x_{min})\,\{\tanh[9\,((i-1)/(B-1) - 0.5)] + 1\} + \Delta x_{min}$ where Δx_{min} and Δx_{max} are the minimum and maximum mesh sizes, B is number of meshes required, and $i = 1, 2, \ldots, B$ is the mesh index.

	For $-0.5 \le x \le 0.5$	For $-0.6 \le x < -0.5$ and $0.5 < x \le 0.6$	For $-1.3 \le x < -0.6$ and $0.6 < x \le 1.3$
Mesh I	$\Delta x = 0.004$	$\Delta x_i = F_i(0.004, 0.02, 12)$	$\Delta x_i = F_i(0.02, 0.1, 13)$
Mesh II	$\Delta x = 0.002$	$\Delta x_i = F_i(0.002, 0.01, 22)$	$\Delta x_i = F_i(0.01, 0.05, 24)$
Mesh III	$\Delta x = 0.001$	$\Delta x_i = F_i(0.001, 0.005, 46)$	$\Delta x_i = F_i(0.005, 0.025, 50)$
	For $x < -1.3$ and $x > 1.3$	For all x	
Mesh I	$\Delta x = 0.1$	$\Delta y = H/50$	
Mesh II	$\Delta x = 0.05$	$\Delta y = H/50$	
Mesh III	$\Delta x = 0.025$	$\Delta y = H/50$	

and $\boldsymbol{W}_{k+1}$ at all panel mesh points are less than the prescribed precision ε, then the final solutions $\boldsymbol{U}_j = \boldsymbol{U}_{k+1}$ and $\boldsymbol{W}_j = \boldsymbol{W}_{k+1}$ are fed to next time step; otherwise $\boldsymbol{U}_k$ and $\boldsymbol{W}_k$ are updated to continue until the precision requirement is reached. Since the direct and feed-back effects between aeroacoustics and panel dynamics are accounted for in every iteration on the same footing, the procedure described leads to a very tightly coupled scheme for resolving the fluid-panel interaction. In all the calculations reported in the present paper, λ and ε were set equal to 0.5 and 10^{-10}, respectively. Normally around 20 iterations were required at each time step.

APPENDIX B: MESH CONVERGENCE

We conduct a convergence study of different mesh designs on the fluid domain and the panel before the actual calculations of all cases reported in the paper. A summary of the mesh designs is given in Table I. One should note that finer mesh sizes are adopted in the vicinity of the panel to suppress the contamination of the truncation errors on the fine details of calculated aeroacoustic-structural interaction as much as possible. The coarser mesh sizes in the rigid duct sections are so selected that the acoustic wave propagation with the fastest mean flow of interest (i.e., $M = 1.2$) can be correctly calculated, yet it does not make the time for calculations prohibitively long. We follow the approach given in Lam *et al.*[25] to set the time step size and fix the CFL number for all mesh designs. For illustrative purposes only, the mesh convergence check with the time-stationary solution of the case $L_p/H = 5$ and $M = 0$ is described here. Figure 12 shows the sensitivity of the resolved temporal of the total acoustic pressure and the panel vibration mobility under the acoustic-structural interaction. Evidently the variation decreases with the mesh size. The maximum deviations in the pressure and mobility obtained from switching from mesh I to mesh II are 2.3% and 0.61%, respectively. Upon switching from mesh II to mesh III, the maximum deviations further reduce to 0.055% and 0.25%, respectively. Therefore we select the mesh II in all calculations reported in previous discussions.

APPENDIX C: VALIDATION FOR AEROACOUSTIC-STRUCTURAL INTERACTION

We choose the experimental study of Choy and Huang[9] on the drum-like silencer carrying a low Mach number flow as the benchmark for our validation. There are two opposing side-branch cavities covered with flexible panels in the silencer design. This configuration is more complex than that in Fig. 1 and thus presents a more stringent case for the validation for coupled AASI. The two-dimensional computational domain of the silencer geometry is shown in Fig. 13. A mesh similar to mesh II in Appendix B is adopted. For our calculation, we take a set of experiment parameters with the test section length 1870 mm, the duct width and cavity height $\hat{H} = 100$ mm, the panel and cavity length $\hat{L}_p = 500$ mm, the mass per unit area of the panel $\hat{\rho}_p \hat{h}_p = 0.17\,\mathrm{kg/m^2}$, the tension $\hat{T}_x = 8213.38\mathrm{N/m}$, and a mean flow of Mach number $M = 0.045$. A broadband incident acoustic plane wave covering 20–1000 Hz is introduced into the computational domain. Its realization in the calculation follows the method proposed in Leung *et al.*[26] with a frequency resolution $\Delta\hat{f} = 10$ Hz.

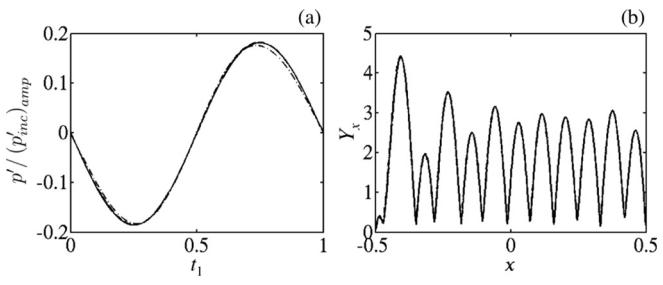

FIG. 12. Sensitivity of numerical solutions to mesh size. (a) Time trace of total acoustic pressure. (b) Panel mobility. –·–·–, mesh I; ———, mesh II; – – –, mesh III.

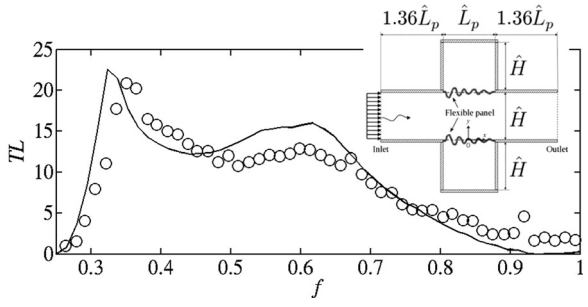

FIG. 13. Comparison between the numerical transmission loss *TL* with experimental data. ———, numerical result; ○, experimental result. The right top corner shows the schematic configuration of the problem.

We use the same numerical settings and normalization as in Sec. II in our calculation. The flow-panel coupling scheme is applied to the two flexible panels and the flows in the main duct and the cavities. A comparison between the calculated transmission loss *TL* with the experimental data is illustrated in Fig. 13. The excellent agreement in the spectral variation of *TL* firmly establishes the capability of the present numerical methodology in capturing AASI correctly. The difference in the *TL* levels may be attributed to two reasons. One is due to the fact that the present two-dimensional calculation may not approximate fully the three dimensionality of the experiment. Some three-dimensional panel vibration and duct acoustic modal behaviours may not be properly included. Another is the assumption of uniform duct flow that excludes any acoustic reactive response due to flow instability driven panel vibration in the experiment. These two issues will be further studied in a later work.

[1]A. Cummings, "Sound transmission through duct walls," J. Sound Vib. **239**, 731–765 (2001).
[2]P. W. Carpenter and A. D. Garrad, "The hydrodynamic stability of flow over Kramer-type compliant surfaces. Part 2. Flow-induced surface instabilities," J. Fluid Mech. **170**, 199–232 (1986).
[3]A. D. Lucey, "The excitation of waves on a flexible panel in a uniform flow," Philos. Trans. Roy. Soc. A. **356**, 2999–3039 (1998).
[4]A. Frendi, L. Maestrello, and L. Ting, "An efficient model for coupling structural vibrations with acoustic radiation," J. Sound Vib. **182**, 741–757 (1995).
[5]L. Huang, "A theoretical study of duct noise control by flexible panels," J. Acoust. Soc. Am. **106**, 1801–1809 (1999).
[6]R. L. Clark and K. D. Frampton, "Aeroelastic structural acoustic coupling: Implications on the control of turbulent boundary-layer noise transmission," J. Acoust. Soc. Am. **102**, 1639–1647 (1997).
[7]F. Schäfer, S. Müller, T. Uffinger, S. Becker, J. Grabinger, and M. Kaltenbacher, "Fluid-structure-acoustic interaction of the flow past a thin flexible structure," AIAA J. **48**, 738–748 (2010).
[8]R. C. K. Leung, H. K. H. Fan, and G. C. Y. Lam, "A numerical methodology for resolving aeroacoustic-structural response of flexible panel," in *Flinovia—Flow Induced Noise and Vibration Issues and Aspects*, edited by E. Ciappi, S. De Rosa, F. Franco, J.-L. Guyader, and S. A. Hambric (Springer, Cham, 2015), pp. 321–342.
[9]Y. S. Choy and L. Huang, "Effect of flow on the drumlike silencer," J. Acoust. Soc. Am. **118**, 3077–3085 (2005).
[10]D. G. Crighton, "Acoustics as a branch of fluid mechanics," J. Fluid Mech. **106**, 261–298 (1981).
[11]G. C. Y. Lam, R. C. K. Leung, S. K. Tang, and K. H. Seid, "Validation of CE/SE scheme for low Mach number direct aeroacoustic simulation," Int. J. Nonlinear Sci. **15**, 157–169 (2014).
[12]G. C. Y. Lam, R. C. K. Leung, and S. K. Tang, "Aeroacoustics of T-junction merging flow," J. Sound Vib. **133**, 697–708 (2013).
[13]S. Choi and Y.-H. Kim, "Sound-wave propagation in a membrane-duct," J. Acoust. Soc. Am. **112**, 1749–1752 (2002).
[14]C. Bogey, "A family of low dispersive and low dissipative explicit schemes for flow and noise computations," J. Comput. Phys. **194**, 194–214 (2004).
[15]S. C. Chang, "The method of space-time conservation element and solution element—a new approach for solving the Navier–Stokes and Euler equations," J. Comput. Phys. **119**, 295–324 (1995).
[16]J. S. Rao, *Dynamics of Plates* (Narosa Publishing House, New Delhi, 1999), 227 pp.
[17]R. Szilard, *Theories and Applications of Plate Analysis: Classical, Numerical, and Engineering Methods* (Wiley and Sons, Hoboken, NJ, 2004), pp. 57–60.
[18]S. I. Hayek, *Advanced Mathematical Methods in Science and Engineering*, 2nd ed. (CRC Press, Boca Raton, FL, 2011), pp. 599–600.
[19]M. de' Michieli Vitturi, T. Esposti Ongaro, A. Neri, M. V. Salvetti, and F. Beux, "An immersed boundary method for compressible multiphase flows: Application to the dynamics of pyroclastic density currents," Computat. Geosci. **11**, 183–198 (2007).
[20]I. Jadic, R. M. C. So, and M. P. Mignolet, "Analysis of fluid-structure interactions using a time-marching technique," J. Fluid. Struct. **12**, 631–654 (1998).
[21]J. W. Miles, "On the generation of surface waves by shear flows. Part 3. Kelvin—Helmholtz instability," J. Fluid Mech. **6**, 583–598 (1959).
[22]L. Huang, "Reversal of the Bernoulli effect and channel flutter," J. Fluid. Struct. **12**, 131–151 (1998).
[23]J. E. John and T. G. Keith, *Gas Dynamics*, 3rd ed. (Pearson Prentice Hall, Upper Saddle River, NJ, 2006), pp. 189–228.
[24]D. A. Anderson, J. C. Tannehill, and R. H. Pletcher, *Computational Fluid Mechanics and Heat Transfer*, 2nd ed. (McGraw-Hill Education, New York, 1984), pp. 156–157.
[25]G. C. Y. Lam, R. C. K. Leung, and S. K. Tang, "Aeroacoustics of duct junction flows merging at different angles," J. Sound Vib. **333**, 4187–4202 (2014).
[26]R. C. K. Leung, R. M. C. So, M. H. Wang, and X. M. Li, "In-duct orifice and its effect on sound absorption," J. Sound Vib. **299**, 990–1004 (2007).